Proceedings of 12th European Conference on Turbomachinery Fluid dynamics & Thermodynamics
ETC12, April 3-7, 2017; Stockholm, Sweden

COMPARISON OF LES AND RANS PREDICTIONS WITH EXPERIMENTAL RESULTS OF THE FAN OF A TURBOFAN

N. Odier - F. Duchaine - L.Y.M Gicquel

CFD Team, CERFACS, 31057 Toulouse, France, odier@cerfacs.fr

G. Dufour - N. García Rosa

Institut Supérieur de l'Aéroanautique et de l'Espace (ISAE-SUPAERO), Université de Toulouse, 31055 Toulouse Cedex 4, France, guillaume.dufour@isae.fr

ABSTRACT

This paper aims at validating LES capability if applied to an actual turbofan configuration at nominal regime, if compared to RANS and experimental measurements. For assessment, averaged radial profiles are compared in 3 axial planes – before the stage, between the rotor blade and stator vanes, and downstream of the stator. RANS and LES results are in very good agreement, but found to be shifted compared to the measurements and for some quantities. An analysis of the unsteady axial velocity is then proposed, investigating root-mean square of axial velocity. Tip-leakage, as well as two boundary layer transitions are evidenced in the rotor. An estimation of the integral turbulent timescale is finally proposed in the whole domain, using autocorrelation of the axial velocity. Suction-side horseshoe vortices are found to be very coherent, as well as the stator corner vortices. Regions of large timescale are moreover evidenced between rotor and stator wakes.

NOMENCLATURE

C_R Rotor chord at midspan
C_S Stator chord at midspan
LE Leading edge
Π_t Total pressure ratio
$P_{i_{2A}}$ Total pressure at station 2A
PS Pressure side
Q mass flowrate
rms Root mean square
R_t Total temperature ratio
R_{uu} Autocorrelation coefficient of $u^{'}$
SS Suction side
$T_{i_{2A}}$ Total temperature at station 2A
t_{turb} Integral turbulent time
$\overline{U}$ Time averaged axial velocity
$u^{'}$ Fluctuating part of axial velocity
$u_{x_{rms}}$ Axial velocity root mean square
$_x$ relative to axial component

INTRODUCTION

Turbomachinery flows are nowadays classically computed with a Reynolds Averaged Navier Stokes (RANS) approach. Its relative low cost and ability to predict global performance with reasonable accuracy at design working point regime makes it popular. This method is also able to go beyond simple global performance prediction with an unsteady formulation (URANS), with predicting unsteady deterministic phenomena. Ottavy et al. (2012) [21] for example validate URANS computations on the 3,5 stage CREATE compressor, and Gourdain et al. (2012) [10] investigate the tip clearance effect on the same compressor, showing that a rotating instability is likely to appear depending on the tip clearance height. In a similar way, Crevel et al. (2014a, 2014b) [4, 5] investigate stall and surge instabilities on the same compressor.

In terms of CFD modelling, Large Eddy Simulation (LES) is particularly well suited to study off-design points and chaotic features such as turbulence. However and because its associated computational cost can be a severe drawback, hybrid RANS/LES are developed for turbomachinery flows. To deal with boundary layers at walls, Spalart et al. (1997) [30] have proposed an alternative method named Detached Eddy Simulation (DES), consisting in solving LES equations in the whole domain except near the walls where boundary layers are computed through a RANS approach. Examples on complex geometries are given in Tucker et al. (2010) [31]. Boudet et al. (2015) [3] have proposed an alternative method relying on zonal LES computation in the tip leakage region of a low-speed fan, allowing the authors to perform a turbulent investigation in the tip-flow, while the flow at inner radii is computed with a classic RANS approach. Riera et al. (2016) [26] investigated the tip flow of the CREATE configuration thanks to a zonal DES and show considerable improvements over both RANS and URANS. If DES is promising, this method still remains challenging in configurations where transition plays a significant role.

Computational cost induced by the large Reynolds numbers involved in a turbomachinery configuration makes pure LES computations quite rare in the literature, in comparison to the existing RANS or hybrid RANS/LES predictions. Hah (2009) [11] is among the first to demonstrate the advantages of a pure LES, clarifying a debated issue regarding flow features in the NASA Rotor 37 and showing evident improvement in total loss predictions. Considering industrial computations, Papadogiannis et al. (2016) [23, 22] validated a wall-modeled LES on a transonic turbine stage, Gourdain (2013) [9] performed a wall-resolved LES on a single-stage axial compressor, and de Laborderie et al. (2016) [6] have presented a wall-modeled LES computation of the 3.5 stages CREATE configuration, taking into account technological effects.

For acoustic predictions — a major issue on a fan configuration — an accurate turbulent prediction is mandatory for any proper broadband noise prediction. An evaluation of the integral turbulent lengthscale is needed for analytical acoustic models like the Amiet (1975) [1] formulation, investigated by Bonneau et al. (2016) [2] using a ZDES approach or the Hanson (2001) model [12] investigated in Leonard et al. (2016) [18] with a LES method. As discussed in Tucker (2013) [32], and Tyacke and Tucker (2015) [33], this specific LES literature is suffering from a lack of high-level validation, such as one-point spectral analysis or two points correlations, both quantities being critical flow characteristics that need to be adequately evaluated for proper quality acoustic predictions.

This paper presents comparisons between LES, RANS, and experiments in a fan stage of an actual turbofan, and shows LES possibilities for investigating the unsteady behavior of the velocity. The latter will be confronted to experimental results in the near future.

DESCRIPTION OF EXPERIMENTAL, RANS AND LES CONFIGURATIONS

Experimental setup : DGEN 380

The fan under study belongs to the world's smallest civil turbofan, the DGEN-380 designed by Price Induction, intended to power personal light jets, and having a 2.5 kN thrust delivery. The fan diameter is less than $352mm$, its rotor has $Zr = 14$ blades and the stator has $Zs = 40$. The present study focuses on the nominal operating point leading to a rotational speed of 10971.6 rpm, and an experimentally measured mass flow of 10.85 kg/s. The chord-based Reynolds numbers are about $Re_R = 700.000$ in the rotor and $Re_S = 322.000$ in the stator. Tests are carried on an instrumented version of the DGEN, presented in Figure 1, where cycle performance is measured thanks to conventional instrumentation. A set of radial intrusion ports complete this setup, allowing the introduction of five-hole probes at different axial and azimuthal positions (see Figure 1). Conventional and specific instrumentation, as well as the mass flow rate measurement methodology, are detailed in García Rosa et al. (2015) [8].

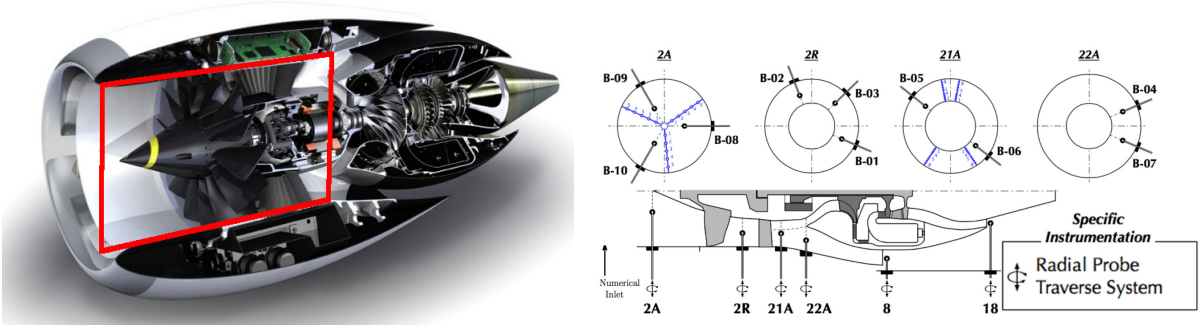

Figure 1: **Illustration of the DGEN-380 (left, courtesy of Price Induction). The fan and its outlet guide vane are evidenced in red. Experimental instrumentation (right).**

RANS: configuration, methodology and numerics

RANS simulations are performed with the Euranus solver of the Fine/Turbo^{TM} package of Numeca. This multi-block solver is thoroughly presented by Hirsch et al (1991) [13]. RANS in the rotating frame are solved with a pseudo-time-marching method. Time integration is ensured by a four-stage Runge-Kutta scheme with implicit residual smoothing. Local time stepping and a three-level multigrid technique are used to accelerate convergence to the steady state. The discretization in space is based on a cell-centered finite-volume approach. Convective fluxes are determined by a second-order centered scheme with added artificial dissipation of the Jameson (1981) type [14]. Second order viscous fluxes are centered. The first cell at the wall has a size of 5 μm, ensuring a value of $y^+ \simeq 1$ over all the blades; the expansion ratio across the boundary layer mesh is approximately 15 %. The complete mesh consists of 11.7 million points. A mixing plane is located between the rotor and the stator, treated with a conservative coupling by pitchwise rows. Turbulence closure is provided by the one-equation model of Spalart and Allmaras. At the inlet of the numerical domain, radial profiles of total quantities are imposed according to the experimental measurements to account for the installation effects. At the core

and bypass duct outlets, static pressure is imposed with a radial equilibrium condition. More details on the mesh and on the validation of the RANS results can be found in Dufour et al (2015) [7].

LES: configuration, methodology and numerics

The compressible Navier-Stokes equations describing the mass, momentum, and energy conservation are solved on an unstructured grid. The fluid follows a perfect gas law $p = \rho r T$ where r is the mixture gas constant, and its dynamic viscosity is varying with temperature according to a power law. Equations are solved using a finite-volume Lax-Wendroff time-explicit scheme, second-order accurate in space and time (Lax Wendroff, (1964))[17]. The unresolved turbulent contributions are modeled with the WALE subgrid model proposed by Nicoud and Ducros (1999) [20]. To numerically deal with the rotor/stator interface in a LES context, the TurboAVBP solver is used. Its methodology, detailed in Wang et al. (2014) [34] relies on the external coupling of two LES computations, the first one being dedicated to the rotor computation, the second to the stator one. Each LES computation is performed with the AVBP solver, detailled in Schønfeld et al. (1999) [28]. The mesh movement in the rotor part is achieved thanks to the ALE method [19], where equations are solved in the absolute frame. The exchange of information from an instance to the other relies on an overset grid method, where conservative variables of an instance are interpolated on nodes belonging to the other one in the overlapping area. The "reduced blade count" technique is applied to the stator part, enabling the computation of a single 360/14-degree periodic sector. This leads to a single rotor blade for three stator vanes. For numerical issues, the computational domain is modified at the outlet to a single duct instead of a flow splitter. The computational domain is depicted in Figure 2. Three computations are performed on meshes composed of 50 millions (M1), 100 millions (M2), and 200 millions (M3) cells, with a 10 prism layer on blades for the most refined mesh, enabling a tip-gap discretisation with 17 cells. For meshes M1 and M2, $x^+ = y^+ = z^+$. Meshes M2 and M3 have the same x^+ and z^+ (of the order of 100, see Figure 3). Only y^+ differs for those last meshes. Computational costs per rotation are 8.000 h CPU for M1, 40.000 h CPU for M2, and 130.000 h CPU for M3. About 6.200 time-steps are needed for a blade passage with M1, 8.500 time-steps with M2, and 15.600 time-steps for M3. Averaged y^+ values at midspan of the rotor and stator blades are depicted in Figure 3 for the three meshes M1, M2 and M3. Wall-law is used to model the boundary layer, with a linear law if y^+ is lower than 11 (Schmitt et al, 2007)[27], logarithmic otherwise. Non-reflecting NSCBC (Poinsot and Lele, 1992) [24] total conditions are imposed at inlet, according to the experimental measurements. Purely axial inflow is imposed at the inlet, as well as no turbulent injection. At this point of the project, measurements of unsteady quantities are not available. Turbulent intensity is expected to be less than 3%, that is measured under windmilling conditions, where very large boundary layers on shroud occur. Freestream turbulence is likely to impact the suction sides boundary layer transition modes, as noticed in Scillitoe et al. [29]. This may have consequences on the averaged profiles, as well as the general working point. As turbulent measurements will be available, a sensibility study will have to be performed. Static pressure is imposed with NSCBC conditions are imposed at outlet, where a radial equilibrium naturally occurs (Koupper et al., 2014) [16]. Static pressure at outlet is adjusted to match the experimental total pressure ratio at station 21A, downstream of the stator. The outlet static pressure adaptation is performed step by step, as the massflow rate and total pressure ratio at station 21A are stabilized.

To assess the convergence of the computations, temporal evolution of mass flow and total

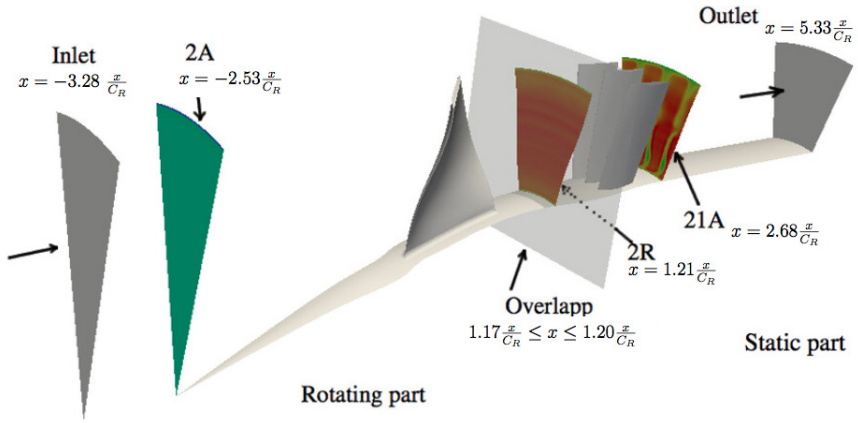

Figure 2: **Computational domain and relative position of planes of interest in terms of rotor blade chord.**

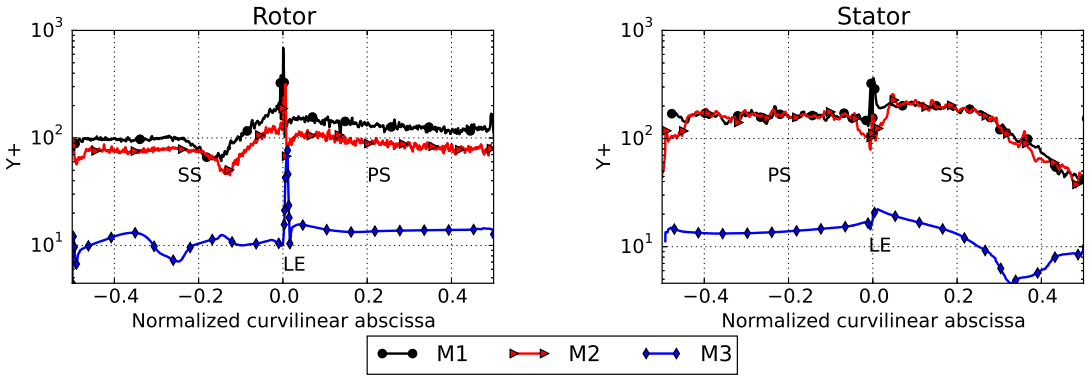

Figure 3: **Averaged y$^+$ values for the 3 LES meshes at midspan of rotor and stator.**

pressure ratio are presented in Figure 4 for the three meshes. Statistics are performed on the last 9 rotor rotations for M1, the last 6 rotations for M2, and the last rotation for M3.

GLOBAL PERFORMANCE COMPARISONS

Figure 5 displays the total pressure ratio and the isentropic efficiency $\eta_{is} = \frac{\Pi_t^{\frac{\gamma-1}{\gamma}}}{R_t - 1}$ along with the reduced massflow $Qred = \frac{Q\sqrt{T_{i_{2A}}}}{P_{i_{2A}}}$, upstream of the rotor (see Figure 1). The aerodynamic map has been obtained through RANS computations. A very good total pressure ratio — that is the targeted value in the numerical approaches — is depicted for both RANS and LES predictions. A 2% overprediction of the mass flowrate is evidenced for numerical results, underlying that losses may be globally underpredicted. This massflow overprediction has also to be linked to the offset observed in static pressure and Mach number in Figure 6 to Figure 8, further discussed. The isentropic efficiency is better predicted through RANS than through LES computations, but LES mesh refinement leads to an increase in the accuracy of the predic-

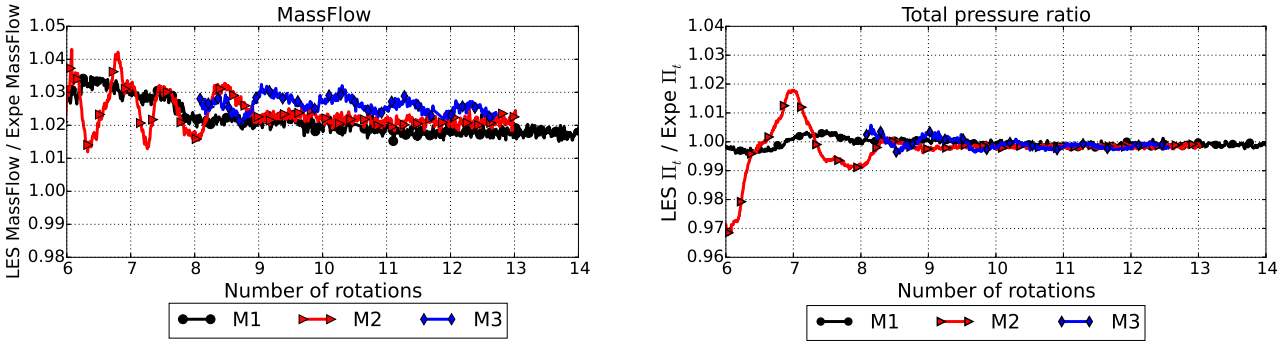

Figure 4: **Mass flow and total pressure ratio temporal evolutions as obtained for the three LES predictions.**

Case	Massflow (kg/s)	Diff. with Expe	Total pressure ratio	Diff. with Expe	Isentropic efficiency	Diff. with Expe
Expe	10.86	0%	1.139	0%	0.8693	0%
RANS	11.18	2.95%	1.144	0.44%	0.8774	0.93%
M1	11.09	2.12%	1.138	-0.08%	0.8378	-3.82 %
M2	11.08	2.03%	1.139	0%	0.8496	-2.26%
M3	11.09	2.12%	1.138	-0.08%	0.8551	-1.63 %

Table 1: **Summary of differences when compared to the experiment for massflow, total pressure ratio, isentropic efficiency, for every configuration.**

tion, and isentropic efficiency with M3 is likely to evolve with increased temporal convergence. Table 1 summarizes the differences with experiments of all configurations. Despite the isentropic efficiency mesh convergence, it is found to differ by 1.6% to 3.8% when compared to the experimental result. Table 2 depicts, for the M1 configuration, the effect of a 0.1% variation in the 3 parameters involved in the evaluation of η_{is}. Up to 2.3% variation is evidenced for a 0.1% variation in one of its parameters. Note that the range of total pressure, total temperature, and γ in the average solution obtained with M1 make Π_t, R_t and γ varies by up to $\pm 8\%$, $\pm 1\%$ and $\pm 0.18\%$ respectively. The sensibility evidenced in Table 2 underlines the need for large margins in the evaluation of η_{is}.

An overall good global performance prediction is finally achieved for both RANS and LES computations.

RADIAL PROFILE COMPARISONS

In this section we turn our attention to the comparison of the time-averaged radial profiles at several stations located respectively upstream of the rotor, downstream of the rotor, and downstream of the stator.

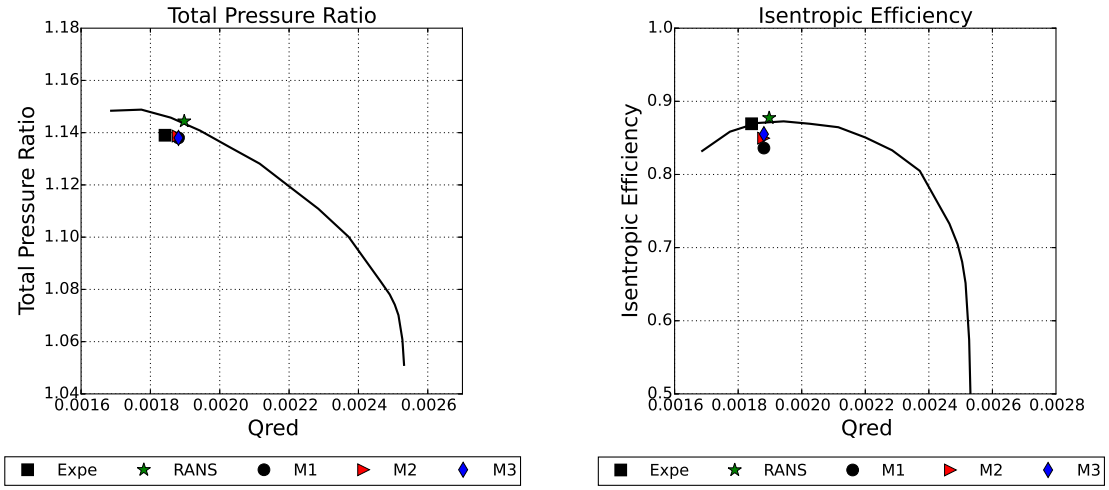

Figure 5: **Fan stage performance: total pressure ratio (left) and isentropic efficiency (right) against reduced mass flow. Aerodynamic map obtained through RANS computations for the considered iso-rotationnal speed is also depicted.**

M1: 0.1% variation in	Resulting variation in $\eta_{is} = \frac{\Pi_t^{\frac{\gamma-1}{\gamma}}}{R_t - 1}$
γ	0.25 %
Π_t	0.8 %
R_t	2.3 %

Table 2: **Effect of a 0.1% variation on parameters involed in η_{is}.**

Rotor intake (Station 2A)

Averaged profiles at station 2A, upstream of the rotor, are displayed in Figure 6. Very good agreement is found between experiments, RANS and LES for total quantities and swirl angle. Both RANS and LES average profiles are found again to be in very good agreement when focusing on Mach number and static pressure profiles. These latter are however found to be slightly shifted with respect to the experimental ones, even if the trends are well reproduced.

Rotor outlet (Station 2R)

Downstream of the rotor, at station 2R, both RANS and LES total pressure ratio and flow angle profiles are found to be in good agreement with measurements as reported in Figure 7. Focusing on static pressure, total temperature and Mach number, both RANS and LES predictions are in fair agreement, and display again an offset when compared to the experimental data. RANS ands LES start to differ in the tip region, when focusing on total temperature and swirl angle. The effect of mesh refinement LES is evidenced in the tip region, where computation on mesh M3 predicts a better swirl angle than with meshes M1 and M2. Despite this mesh refinement, the M3 mesh remains unable to be in an exact agreement in the tip region

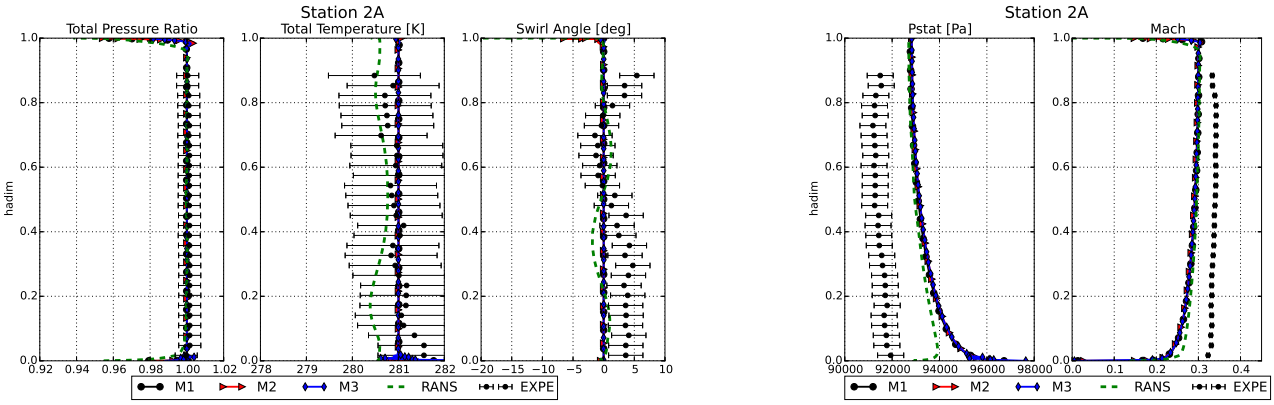

Figure 6: **Profiles upstream of the rotor (station 2A).**

for the swirl angle, underlying the need for a more refined computation in this region.

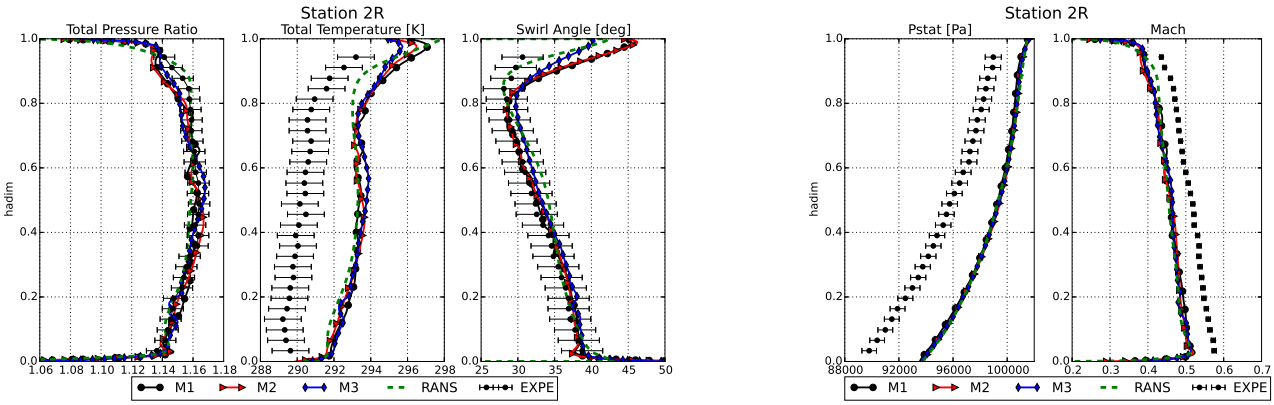

Figure 7: **Profiles downstream of the rotor (station 2R).**

Stator outlet (Station 21A)

Similar conclusions can be drawn downstream of the stator, at station 21A. Figure 8 indeed depicts the same agreement between numerical results, and the same shift with measurements for corresponding profiles. The LES mesh refinement nonetheless displays more variations than for the previously discussed LES profiles, underlying the need for a more refined computation.

UNSTEADY FLOW FEATURE ANALYSIS

Going beyond the averaged results presented above, an investigation of the unsteady axial velocity is performed in this section. For this specific analysis, the velocity u is decomposed into its time averaged and fluctuating components, respectively noted $\overline{U}$ and $u^{'}$:

$$u(x,t) = \overline{U(x)} + u^{'}(x,t) \tag{1}$$

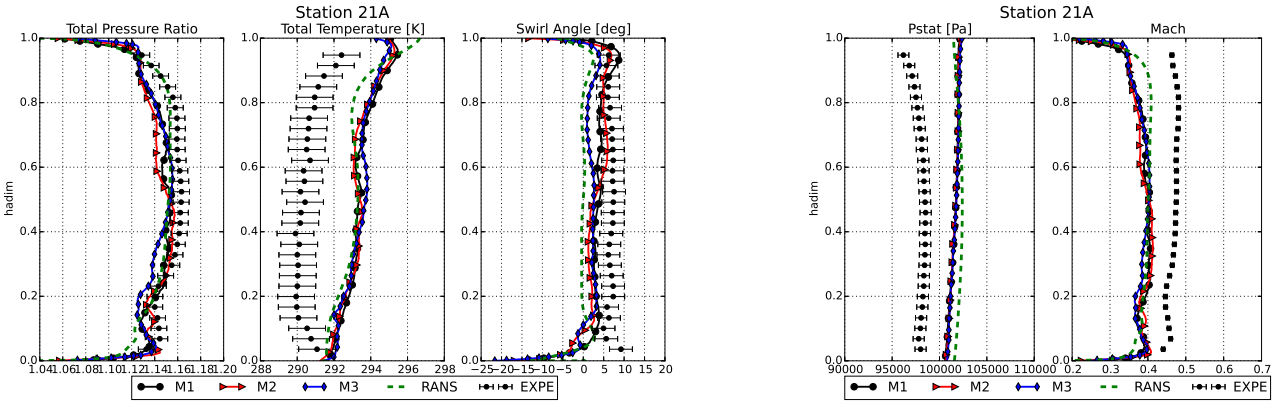

Figure 8: **Profiles at station 21A, downstream of the stator.**

where the time-averaged velocity is approximated by

$$\overline{U} = \frac{1}{N}\sum_{i=1}^{N} u_i \tag{2}$$

if N is the number of samples. The axial velocity root mean square yields:

$$u_{x_{rms}} = \sqrt{\frac{1}{N}\sum_{i=1}^{N}(u_{x_i} - \overline{U})^2} \tag{3}$$

Note that our current work is nowadays devoted to account for the deterministic fluctuation due to the rotation. Root mean square of axial velocity $u_{x_{rms}}$ on mesh M3, given by statistics over the analysed time, is plotted in Figure 9 in the relative rotor frame for four axial planes, as well as an instantaneaous contour of Q-criterion –from an arbitrary instantaneaous solution– colored by the local Mach number value. This specific iso-Q contour materializes the tip leakage vortex (I), a significant horseshoe vortex leg (II), as well as two boundary layer separations (III) on the blade suction side. The first and last feature induce large $u_{x_{rms}}$ values at casing (I) and suction side (III), whereas the horseshoe vortex leg (II) could not be exhibited throught the level of $u_{x_{rms}}$. The decreasing values of $u_{x_{rms}}$ in the rotor wake downstream of the trailing edge evidences its turbulent diffusion. For meshes M1 and M2, levels of $u_{x_{rms}}$ are very similar to those obtained on M3, but the boundary layer separation on the suction side is not evidenced (not shown).

This analysis is performed in the stator domain, as illustrated in Figure 10. Contours of Q-criterion depict the remaining components of the wake coming from the rotor trailing edge (IV), and from the tip-leakage wake (V). On the stator suction side, a transition of the boundary layer is observed (VII), as well as a corner-vortex (VIII). In the absolute frame, vortices coming from rotor wakes induce quite significant values of $u_{x_{rms}}$ upstream of the stator. The horseshoe vortex is also seen to perturb the flow in the absolute frame at a very identifiable radius (VI). Values of $u_{x_{rms}}$ slightly decrease within the first half of the stator chord until the boundary layer transition occurs. This flow separation indeed leads to high fluctuation levels on the suction side. A large level of fluctuations is finally evidenced in the stator vortex shedding, illustrating

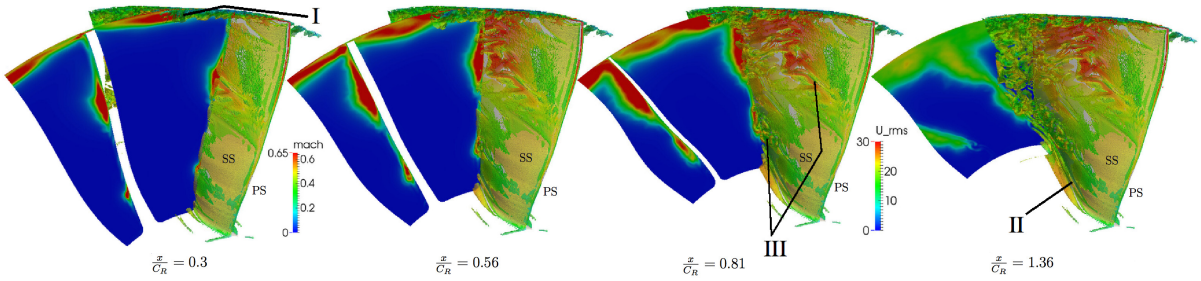

Figure 9: **Evolution of $u_{x_{rms}}$ along the axis in the rotor domain and an arbitrarily chosen instantaneous contour of Q-Criterion colored by the local Mach number value.**

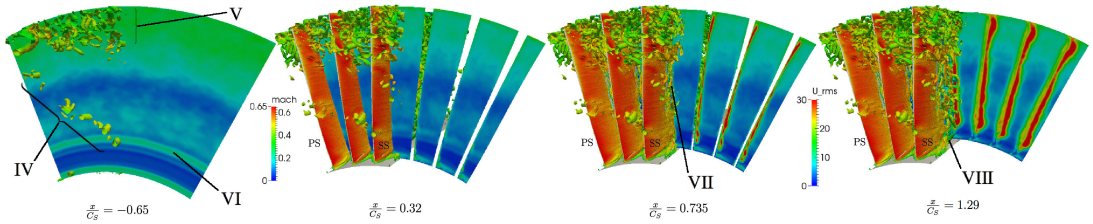

Figure 10: **Evolution of $u_{x_{rms}}$ along the axis in the stator domain and an arbitrarily chosen instantaneous contour of Q-Criterion colored by the local Mach number value.**

its unsteady nature.

As discussed in the introduction, integral turbulent quantities are needed for acoustic analytical models and are numerically estimable only through LES. Those quantities can be estimated by autocorrelation of the velocity fluctuation $u^{'}$:

$$R_{uu}(\tau) = \frac{\overline{u'(t)u'(t+\tau)}}{u_{rms}^2} \, , \tag{4}$$

integral turbulent time being defined as (Pope (2000)) [25]:

$$t_{turb} = \int_{\tau=0}^{\infty} R_{uu}(\tau) \mathrm{d}\tau \, . \tag{5}$$

For actual flows, this integral may not converge, and an infinite computation is not possible. Turbulent timescale is thus obtained by integrating R_{uu} until it reaches an arbitrary threshold, chosen $R_{uu} = 0.5$ in the present study, beyond which the signal is considered not correlated anymore. This choice leads to an underestimation of t_{turb} in the present study compared to the definition given in Eq. 5, but has no impact on its spatial distribution. This methodology has been applied by Koupper et al. (2015) [15] at the exit of a combustor, and gave good agreement between LES and experiment. The following results give an idea of the topology of turbulent eddies in the present flow. Total time of signal used for this analysis corresponds to 25 rotor blade passages. A convergence study has been performed to confirm that the evaluation of the integral timescale does not depend on the sampling frequency, between $12kHz$ and $97kHz$. The following results have been obtained with a sampling frequency of $97kHz$. For comparison,

the Blade Passing Frequency (BPF) is $2.5kHz$. Resulting integral turbulent time is displayed in Figure 11, and shows as expected low turbulent times where high $u_{x_{rms}}$ values were observed in Figure 9. A coherent region is moreover evidenced in the very near field of the tip-leakage wake (IX), convected downstream between the two neighbouring trailing edge wakes. The horseshoe vortex is found to be very coherent (circled in red), unlike the two boundary layer separations occurring on the suction side.

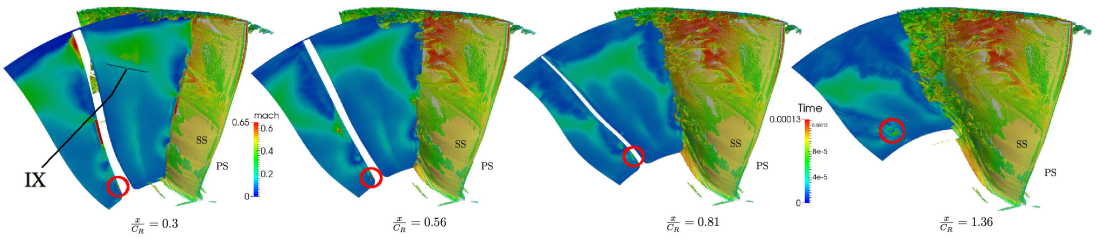

Figure 11: **Evolution of integral turbulent timescale along the axis in the rotor, and an arbitrarily chosen instantaneous contour of Q-Criterion colored by the local Mach number value.**

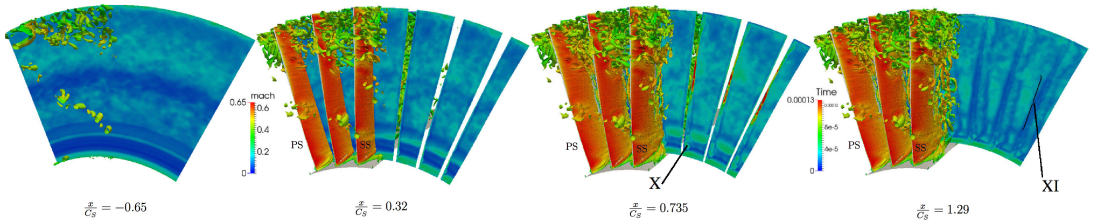

Figure 12: **Evolution of integral turbulent timescale along the axis in the stator, and an arbitrarily chosen instantaneous contour of Q-Criterion colored by the local Mach number value.**

As pointed out in Figure 12, the horseshoe vortex found very coherent in the rotor frame induces an uncorrelated region upstream of the stator leading edge because of its rotating motion. Inside the stator vane, the swirl angle is reduced to reach a quasi zero value (see profiles in Figure 8) and coherence is found again. The corner vortex is also found to be coherent (X), while other coherent regions are found between two neighbouring turbulent wakes (XI). Experimental data is currently awaited for comparison.

CONCLUSIONS

A comparative study between RANS, LES and experimental measurements in an actual turbofan at nominal regime has been carried out. Comparisons of average profiles for three axial positions depict a reasonable agreement between RANS and LES for all results. An offset is however evidenced when numerical total temperature, Mach number, and static pressure are compared to experimental profiles, and remains to be explained. The shape of numerical profiles is nonetheless consistent with experimental results. An investigation of the unsteady axial

velocity is then detailed. In the rotor domain, root mean square of axial velocity materializes the tip-leakage flow and two boundary layer separations on the suction side. In the stator domain, a transition in the suction side boundary layer is evidenced as well as highly unsteady wakes. Integral turbulent timescale shows the potential of LES to provide integral data for acoustic analytical models for which empirical data is generally used. Low integral turbulent timescales are found in regions of high fluctuating velocities. Coherent regions are identified near the tip-leakage, in the horseshoe suction side vortex leg as well as in the stator corner vortex, and between the stator wakes. Integral turbulent database has been numerically obtained in an actual turbomachinery configuration, experimental data being currently awaited for comparison.

ACKNOWLEDGEMENTS

The authors wish to acknowledge the support of the STAE foundation via the RTRA project SIMACO3FI. The computational resources were provided by the GENCI network, and were part of the allocation no. x20162a6074 (CINES-OCCIGEN). Authors also wish to acknowledge Price Induction for providing support.

REFERENCES

[1] R.K. Amiet. Acoustic radiation from an airfoil in turbulent stream. *Journal of Sound and Vibration*, 41:407–420, 1975.

[2] V. Bonneau, C. Polacsek, L. Castillon, and J. Marty. Turbofan broadband noise predictions using a 3D ZDES rotor blade simulation. In *22nd AIAA/CEAS Aeroacoustics Conference*, Lyon, France, 2016. AIAA Papers.

[3] J. Boudet, A. Cahuzac, P. Kausche, and M.C. Jacob. Zonal Large-Eddy Simulation of a Fan Tip-Clearance Flow, With Evidence of Vortex Wandering. *Journal of Turbomachinery*, 137(6):061001, 2015.

[4] F. Crevel, N. Gourdain, and S. Moreau. Numerical simulation of aerodynamic instabilities in a multistage high-speed high-pressure compressor on its test-rig part I: Rotating Stall. *Journal of Turbomachinery*, 136(10):101003, 2014.

[5] F. Crevel, N. Gourdain, and X. Ottavy. Numerical simulation of aerodynamic instabilities in a multistage high-speed high-pressure compressor on its test-rig part II: Deep surge. *Journal of Turbomachinery*, 136(10):101004, 2014.

[6] J. De Laborderie, F. Duchaine, O. Vermorel, L. Gicquel, and S. Moreau. Application of an overset grid method to the large eddy simulation of a high-speed multistage axial compressor. In *ASME Turbo Expo*, GT2016-56344, Seoul, South Korea, 2016.

[7] G. Dufour, N. García Rosa, and S. Duplaa. Validation and flow structure analysis in a turbofan stage at windmill. *Proceedings of the Institution of Mechanical Engineers, Part A: Journal of Power and Energy*, 229(6):571–583, 2015.

[8] N. García Rosa, G. Dufour, R. Barènes, and G. Lavergne. Experimental Analysis of the Global Performance and the Flow Through a High-Bypass Turbofan in Windmilling Conditions. *Journal of Turbomachinery*, 137(5):051001, 2015.

[9] N. Gourdain. Validation of large-eddy simulation for the prediction of compressible flow in an axial compressor stage. In *ASME Turbo Expo*, GT2013-94550, San Antonio, Texas, USA, 2013.

[10] N. Gourdain, F. Wlassow, and X. Ottavy. Effect of Tip Clearance Dimensions and Control of Unsteady Flows in a Multi-Stage High-Pressure Compressor. *Journal of Turbomachinery*, 134(5):051005, 2012.

[11] C. Hah. Large Eddy Simulation Of Transonic Flow Field In NASA Rotor 37. In *47th Aerospace Sciences Meeting*, 2009-215627, Orlando, Florida, 2009.

[12] B. Hanson. Theory Stator Inflow of Lean for Broadband Cascades Turbulence and Sweep With Noise of Rotor Effects and Inhomogeneous Including Effects of Lean and Sweep. Technical Report May, NASA-CR-210762, NASA, East Hartford, Connecticut, USA, 2001.

[13] C. Hirsch, C. Lacor, and C. Dener. An integrated CFD system for 3D turbomachinery applications. Technical report, AGARD-CP-510, 1991.

[14] A. Jameson, W. Schmidt, and E. Turkel. Numerical solutions of the Euler equations by finite volume methods using Runge-Kutta time-stepping schemes. In *AIAA 14th fluid and plasma dynamic conference*, 81-1259, 1981.

[15] C. Koupper, L.Y.M Gicquel, F. Duchaine, T. Bacci, B. Facchini, A. Picchi, L. Tarchi, and G. Bonneau. Experimental and Numerical Calculation of Turbulent Timescales at the Exit of an Engine Representative Combustor Simulator. *Journal of Engineering for Gas Turbines and Power*, 138(2):021503, 2015.

[16] C. Koupper, T. Poinsot, L.Y.M Gicquel, and F. Duchaine. Compatibility of Characteristic Boundary Conditions with Radial Equilibrium in Turbomachinery Simulations. *AIAA Journal*, 52(12):2829–2839, 2014.

[17] P.D. Lax and B. Wendroff. Difference schemes for hyperbolic equations with high order of accuracy. *Commun. Pure Appl. Math*, pages 381–398, 1964.

[18] T. Leonard, M. Sanjose, S. Moreau, and F. Duchaine. Large Eddy Simulation of a scale-model turbofan for fan noise source diagnostic. In *22nd AIAA/CEAS Aeroacoustics Conference*, 2016-3000, Lyon, France, 2016.

[19] V. Moureau, G. Lartigue, Y. Sommerer, C. Angelberger, O. Colin, and T. Poinsot. Numerical methods for unsteady compressible multi-component reacting flows on fixed and moving grids. *Journal of Computational Physics*, 202(2):710–736, 2005.

[20] F. Nicoud and F. Ducros. Subgrid-scale stress modelling based on the square of the velocity gradient tensor. *Flow, Turbulence and Combustion*, 62(3):183–200, 1999.

[21] X. Ottavy, N. Courtiade, and N. Gourdain. Experimental and Computational Methods for Flow Investigation in High-Speed Multistage Compressor. *Journal of Propulsion and Power*, 28(6):1141–1155, 2012.

[22] D. Papadogiannis, F. Duchaine, L.Y.M Gicquel, G. Wang, and S. Moreau. Effects of Subgrid Scale Modeling on the Deterministic and Stochastic Turbulent Energetic Distribution in Large-Eddy Simulations of a High-Pressure Turbine Stage. *Journal of Turbomachinery*, 138(9):10, 2016.

[23] D. Papadogiannis, F. Duchaine, F. Sicot, L. Gicquel, G. Wang, and S. Moreau. Large eddy simulation of a high pressure turbine stage: Effects of sub-grid scale modeling and mesh resolution. In *ASME Turbo Expo*, GT2014-25876, Dusseldorf, Germany, 2014.

[24] T. J. Poinsot and S. K. Lele. Boundary conditions for direct simulations of compressible viscous flows. *Journal of Computational Physics*, 101(1):104–129, 1992.

[25] S Pope. *Turbulent Flows*. Cambridge University Press, 2000.

[26] W. Riéra, J. Marty, L. Castillon, and S. Deck. Zonal Detached-Eddy Simulation Applied to the Tip-Clearance Flow in an Axial Compressor. *AIAA Journal*, pages 1–15, 2016.

[27] P. Schmitt, T. Poinsot, B. Schuermans, and K.P. Geigle. Large-eddy simulation and experimental study of heat transfer, nitric oxide emissions and combustion instability in a swirled turbulent high-pressure burner. *Journal of Fluid Mechanics*, 570:17–46, 2007.

[28] T. Schønfeld and M. Rudgyard. Steady and unsteady flows simulations using the hybrid flow solver avbp. *AIAA Journal*, 37:1378–1385, 1999.

[29] A.D. Scillitoe, P.G. Tucker, and P. Adami. Numerical investigation of the three-dimensional separation in an axial flow compressor: The influence of free-stream turbulent intensity and endwal boundary layer state. In *ASME Turbo Expo*, GT2016-57241, Seoul, South Korea, 2016.

[30] P. R. Spalart, W-H. Jou, M. L. Strelets, and S. R. Allmaras. Comments on the feasibility of LES for wings, and on a hybrid RANS/LES approach. In *Proceedings of the First AFOSR International Conference on DNS/LES*, Ruston, Louisiana, USA, 1997.

[31] P. Tucker, S. Eastwood, C. Klostermeier, J. Jefferson-Loveday, Rand Tyacke, and Y. Liu. Hybrid LES Approach for Practical Turbomachinery Flows: Part 2—Further Applications. *Journal of Turbomachinery*, 134(2):021024–021024–10, 2011.

[32] P.G. Tucker. *Unsteady Computational Fluid Dynamics in Aeronautics*. Springer, 2013.

[33] J. C. Tyacke and Paul G. Tucker. Future use of Large Eddy Simulation in aeroengines. *Journal of Turbomachinery*, 137:081005–1–081005–15, August 2015.

[34] G. Wang, F. Duchaine, D. Papadogiannis, I. Duran, S. Moreau, and L.Y.M Gicquel. An overset grid method for large eddy simulation of turbomachinery stages. *Journal of Computational Physics*, 274:333–355, 2014.